Redox Biology 61 (2023) 102654

Contents lists available at ScienceDirect

Redox Biology

journal homepage: www.elsevier.com/locate/redox

The calcium channel modulator 2-APB hydrolyzes in physiological buffers and acts as an effective radical scavenger and inhibitor of the NADPH oxidase 2

Ewa Jasmin Slowik [a], Katerina Stankoska [a], Nhat Nguyen Bui [a], Bastian Pasieka [a], David Conrad [a,b], Josef Zapp [c], Markus Hoth [a], Ivan Bogeski [d], Reinhard Kappl [a,*]

[a] Department of Biophysics, Faculty of Medicine, Center for Integrative Physiology and Molecular Medicine (CIPMM), Saarland University, 66421, Homburg, Germany
[b] Department of Anaesthesiology, Intensive Care and Pain Therapy, Saarland University Medical Center, Saarland University Faculty of Medicine, 66421, Homburg, Germany
[c] Department of Pharmaceutical Biology, Saarland University, 66123, Saarbrücken, Germany
[d] Molecular Physiology, Department of Cardiovascular Physiology, UMG, 37073, Göttingen, Germany

ARTICLE INFO

Keywords:
2-APB
Ca-signaling
Reactive oxygen species (ROS)
Hydrolysis
Degradation
NOX inhibition

ABSTRACT

2-aminoethoxydiphenyl borate (2-APB) is commonly used as a tool to modulate calcium signaling in physiological studies. 2-APB has a complex pharmacology and acts as activator or inhibitor of a variety of Ca^{2+} channels and transporters. While unspecific, 2-APB is one of the most-used agents to modulate store-operated calcium entry (SOCE) mediated by the STIM-gated Orai channels. Due to its boron core structure, 2-APB tends to readily hydrolyze in aqueous environment, a property that results in a complex physicochemical behavior. Here, we quantified the degree of hydrolysis in physiological conditions and identified the hydrolysis products diphenylborinic acid and 2-aminoethanol by NMR. Notably, we detected a high sensitivity of 2-APB/diphenylborinic acid towards decomposition by hydrogen peroxide to compounds such as phenylboronic acid, phenol, and boric acid, which were, in contrast to 2-APB itself and diphenylborinic acid, insufficient to affect SOCE in physiological experiments. Consequently, the efficacy of 2-APB as a Ca^{2+} signal modulator strongly depends on the reactive oxygen species (ROS) production within the experimental system. The antioxidant behavior of 2-APB towards ROS and its resulting decomposition are inversely correlated to its potency to modulate Ca^{2+} signaling as shown by electron spin resonance spectroscopy (ESR) and Ca^{2+} imaging. Finally, we observed a strong inhibitory effect of 2-APB, i.e., its hydrolysis product diphenylborinic acid, on NADPH oxidase (NOX2) activity in human monocytes. These new 2-APB properties are highly relevant for Ca^{2+} and redox signaling studies and for pharmacological application of 2-APB and related boron compounds.

1. Introduction

The membrane-permeable boron compound 2-APB (2-aminoethoxydiphenyl borate) is commonly used to investigate physiological functions and biophysical properties of several types of Ca^{2+} channels. The pharmacology of 2-APB is rather complex. 2-APB was described to enhance transient receptor potential (TRP) TRPV1-4 and TRPV6 channel activity [1–3], and to inhibit TRPC1/3/4/6/7 and distinct TRPM type channels [4–7]. Moreover, 2-APB is recognized as an inhibitor of inositol 1,4,5-trisphosphate (IP3) receptors [8,9], and as a modulator of the STIM-gated ORAI channels, i.e., the store-operated Ca^{2+} entry (SOCE), depending on its concentration. Applied doses <5 μM enhance SOCE and thus I_{CRAC} (Ca^{2+} release-activated Ca^{2+} current [10]) whereas at doses >20–30 μM, 2-APB inhibits I_{CRAC} in various cell lines [11–14]. Despite its limited selectivity and complex pharmacology, 2-APB is a prototype compound for investigating physiological and biophysical properties of SOCE. In view of the enormous importance of Ca^{2+} signals for proper cellular function [5,15], great efforts have been made in developing specific channel inhibitors/activators based on the 2-APB structure motif. Modifications were introduced at the aminoethoxy- and the

Abbreviations: MC, human monocyte; NOX, NADPH oxidase; SOCE, store operated calcium entry; ESR, electron spin resonance spectroscopy; NMR, nuclear magnetic resonance; DPBAc, diphenylborinic acid; PBAc, phenylboronic acid; BAc, boric acid; 2-AE, 2-aminoethanol.

* Corresponding author.
E-mail address: reinhard.kappl@uni-saarland.de (R. Kappl).

https://doi.org/10.1016/j.redox.2023.102654
Received 28 December 2022; Received in revised form 20 February 2023; Accepted 2 March 2023
Available online 4 March 2023

phenyl-groups for mono- as well as bis-boronate compounds, some of which showed increased specificity and activity for modulation of SOCE and TRP channels [15–22]. Notably, one study on 2-APB and analogue compounds showed evidence for hydrolysis of 2-APB in aqueous buffers. The authors pointed out that this property is largely ignored in physiological experiments [21]. Further evidence for 2-APB hydrolysis was found in a later study on TRPV channels [23].

Calcium signaling via SOCE is a key event in activation of immune cells and in regulating other functions in both, non-excitable and excitable cellular systems. In immune cells specifically, binding of hormones, messengers, antigens, or pathogen-associated molecular patterns to cell specific surface receptors (G protein- and srk tyrosine kinase-coupled receptors) produces IP_3 which induces release of Ca^{2+} from the endoplasmic reticulum (ER) upon binding to ER-located IP_3 receptors. The depletion of ER stores activates ER-located Ca^{2+}-sensing stromal interaction molecules (STIM1 and 2) which interact with Orai channels (Orai1 to 3) at the plasma membrane to finally activate I_{CRAC} and Ca^{2+} flux into the cytosol [10,15]. Depending on the immune cell type, the sustained Ca^{2+} entry elicits a variety of responses such as proliferation, gene expression, secretion, cytokine release, phagocytosis, adhesion, or production of reactive oxygen species (ROS) [24,25]. In addition, TRP channels were suggested to mediate Ca^{2+} influx via a non-SOCE mechanism [25,26].

As a first line of immune defense, professional phagocytes like neutrophils, monocytes (MCs) and macrophages produce large amounts of ROS via the NADPH oxidase 2 (NOX2), a process called “oxidative burst”. This enzyme is located at the plasma and/or phagosome membrane and transfers electrons through the membrane to oxygen in the extracellular space and phagosome lumen, respectively. The electrons originate from the reductive equivalent NADPH. The NOX2 activation process is strictly Ca^{2+}-dependent and requires protein kinases (PKC) and accessory cytosolic proteins for correct assembly of the enzyme [27,28]. NOX2 generates superoxide radicals ($O_2^{\bullet-}$) which are subsequently dismutated to hydrogen peroxide (H_2O_2) and released within the phagosome or into the extracellular medium to mediate bacterial killing and host defense. In a previous study, our group showed that in primary human MCs, bacterial peptides activate SOCE which in turn controls ROS production by NOX2. In a feedback loop, ROS also differentially affected SOCE depending on the Orai1/Orai3 subunit composition of the CRAC-channels [29,30].

Pharmacological tools that modulate SOCE and NOX2 as well as tissue redox state have a high therapeutic potential in treating, among others, autoimmune diseases, hyper-inflammation, cancer, or cardiovascular diseases. Accordingly, it is important to understand if and how the activity of such modulators is regulated or affected by the local tissue environment in order to optimize their clinical application. Based on its chemical structure, we hypothesized that 2-APB pharmacology is complex and might be regulated by environmental redox signals. Our findings suggest that oxidation diminishes the pharmacological effects of 2-APB on SOCE. Furthermore, we demonstrate that 2-APB can act as a potent free radical scavenger and as an inhibitor of NOX2.

2. Materials and methods

2.1. Materials

All chemicals and reactants were purchased from Sigma if not stated otherwise. Stock solutions of 2-APB at 50 or 200 mM were prepared in DMSO or DMSO-d_6 for cell and NMR experiments, respectively, and were further diluted to desired concentrations in aqueous media; phenylboronic acid (PBAc), hydrolyzed diphenylborinic anhydride, i.e., diphenylborinic acid (DPBAc), boric acid (BAc), 2-aminoethanol (2-AE), phenol (Ph), and hydrogen peroxide (30 wt%) were used without further purification. For NMR 0.2 M deuterated phosphate buffer in D_2O (d-PB) with formal pH 7.4 was composed by mixing appropriate amounts of Na_2DPO_4 and KD_2PO_4 salts. For cell experiments, a modified Ringer solution with a composition (in mM) 145 NaCl, 4 KCl, 1 (or as indicated) $CaCl_2$, 2 $MgCl_2$, 10 HEPES, 10 glucose was used; nominally Ca-free buffer contained 1 mM EGTA. For calcium imaging experiments the Ca^{2+}-sensitive dye Fura-2-AM (Invitrogen, 1 mM in DMSO) was used.

2.2. NMR-experiments: spiking and peroxide reaction

NMR spectra were recorded at 298 K using Bruker NMR spectrometers (Bruker BioSpin GmbH, Ettlingen, Germany). For ^1H (500.13 MHz) an Avance III 500, equipped with a 5 mm TXI cryoprobe, was used. ^{11}B NMR (160.46 MHz) and DOSY measurements were performed on Avance I 500, equipped with a BBO probe. All samples were measured in 5 mm NMR tubes from Deutero (Kastellaun, Germany), made either of borosilicate (Boro500-5-7) or, for ^{11}B NMR, of non-boron-containing silica glass (Qtz500-5-7) to minimize boron signals from the glass background. All pulse programs for data acquisition were taken from the standard pulse program library of the corresponding device’s own Topspin version. In particular, the determination of diffusion coefficients with the pulsed field gradient stimulated echo sequence with bipolar gradients and longitudinal eddy current delay is mentioned here (‘ledbpgp2s′ in the library). NMR processing was performed with Bruker’s TS 4.0.5. 2D DOSY spectra with chemical shifts on the F2 axis and diffusion constants on the F1 axis were further generated with Bruker’s Dynamics Center 2.7.1. ^1H spectra were calibrated to residual DMSO (d_H 2.50 ppm) when measured in pure DMSO-d_6. For D_2O solutions, capillaries filled with DMSO-d_6 were used for referencing. ^{11}B NMR spectra were calibrated relative to boric acid (d_B −0.05 ppm, for details see Suppl. Fig. 4). In spiking experiments, the total sum of integrals was set to total proton count of input molecules, i.e., 14 H for 2-APB, 24 H for 2-APB + DPBAc (equimolar), 19 H for 2-APB + PBAc (equimolar), 24 H for 2-APB + Ph (molarity of Ph = 2 • [2-APB]). For the peroxide reaction, 2-APB was dissolved in DMSO-d_6, diluted in buffer to the desired concentration and thoroughly mixed, then corresponding concentrations of H_2O_2 were added. Freshly prepared samples were measured within 10 min after mixing. For hydrolysis experiments, aliquots of 2-APB in DMSO-d_6 were added to different preset D_2O/DMSO-d_6 mixtures to yield the desired concentration and various DMSO-d_6 contents. NMR measurement started ca. 5 min after preparation.

2.3. Cell culture of Jurkat T cells and preparation of primary human monocytes

Research carried out for this study with human material has been approved by the local ethics committee (84/15; Prof. Dr. Rettig-Stürmer). The local blood bank within the Institute of Clinical Hemostaseology and Transfusion Medicine at Saarland University Medical Center provided leukocyte reduction system (LRS) chambers, a by-product of platelet collection from healthy blood donors. All blood donors provided written consent to use their blood for research purposes. Jurkat T cells (Clone E6.1, ATCC, TIB-152) were cultivated in RPMI medium (Thermo Fisher Scientific, +10% (v/v) FCS (fetal calf serum), 100 U/mL penicillin (P), 100 μg/mL streptomycin (S)) at 37 °C (5% CO_2). Primary human MCs were prepared from peripheral blood mononuclear cells (PBMCs). PBMCs were isolated from leukocyte-reducing system (LRS) chambers by density centrifugation. 300 Mio PBMCs were seeded per 750 ml flask (RPMI + 10% FCS + P/S). After 2 h, the medium was renewed to remove the bulk of non-adherent cells. Adhering MCs were then washed with PBS (+0.5% v/v BSA) and incubated with PBS for 10 min at 37 °C under cell culture conditions. The supernatant was collected, cells were detached by scraping and hitting the flask and collected in PBS. Residual adhered cells were incubated with PBS for 5 min at 37 °C and collected. All collected cells were centrifuged (200×*g*, 15 °C, 8 min) and seeded in ultra-low protein binding plates in medium (4 Mio/mL). Cells were measured 1–2 days after isolation to minimize pre-activation.

2.4. Calcium imaging

Jurkat T cells were loaded with 1 μM membrane-permeable Fura-2-AM in RPMI (+10% FCS + P/S, 10 mM HEPES) for 20–30 min at RT and seeded in modified Ringer solution containing 0.5 mM $CaCl_2$ on poly-L-ornithine-coated 25 mm coverslips. Cells were perfused with modified Ringer solution containing 0.5 mM $CaCl_2$ or Ca-free solution supplemented with the mentioned substances at indicated times. ER stores were depleted and SOCE was induced by adding 1 μM thapsigargin (Tg, diluted in DMSO; blocker of the SERCA pumps). Live cell imaging (at 37 °C) was performed using a Zeiss inverse microscope, Polychrome V (TILL Photonics) light source and Clara CCD camera (Andor). F76-521 Fura-2 HC filter cubes (AHF Analysetechnik AG) were used for excitation of Fura-2 loaded samples at 340 nm and 380 nm. Images were acquired at 0.2 Hz with 25 ms exposure time. Images were background corrected and resulting ratio images ($F_{340/380}$) were analyzed to detect changes in cytosolic Ca^{2+}.

2.5. NOX-2 activation, superoxide formation and oximetry measured by electron spin resonance (ESR) spectroscopy

Primary human MCs were washed and resuspended in modified Ringer solution with 1 mM $CaCl_2$, supplemented with 25 μM deferoxamine methane sulfonate salt (Noxygen, NOX-09.1) and 5 μM diethyldithiocarbamic acid sodium salt (Noxygen, NOX-10.1). MCs were counted using the curve-fit tool (MoxiZ, Corning). Generally, 0.35–0.6 Mio MCs were used for simultaneous measurement of superoxide production and oxygen consumption by ESR. To the pre-set volume of cell suspension, the following reagents were added: 1 μM trityl (tetrathiatriarylmethyl solution, Noxygen) to detect oxygen content, 300 μM CMH (1-hydroxy-3-methoxycarbonyl-2,2,5,5-tetramethylpyrrolidine, Noxygen), 1 μM phorbol-12-myristat-13-acetat (PMA), 1 μM thapsigargin (Tg), 2 μM ionomycin (Iono) and 2-APB/DPBAc/PBAc as desired. For ROS sample preparation, the sequence of additions was: buffer + MCs + (trityl) + (2-APB/DPBAc/PBAc) + CMH + PMA/Tg/Iono; the substances in parentheses were added according to the experiment design. The final 50 μL sample was resuspended, transferred to a glass capillary (Ringcaps®, Noxygen) and sealed with Critoseal (Noxygen). The capillary was quickly (within 1 min) inserted into the quartz finger at 37 °C controlled by a temperature & gas controller BIO-III (Noxygen). ESR spectra were recorded with a Bruker ESP300e spectrometer equipped with a ST9010 cavity. Spectrometer settings were for microwave attenuation 10 dB (= 20 mW microwave power), modulation amplitude 0.07 mT, modulation frequency 100 kHz, receiver gain 60 dB, conversion time 60 ms, time constant 20 ms, center field 346.6 mT, sweep width 6.0 mT; the microwave frequency was measured with a HP 5010 frequency counter.

Spectra were recorded every minute and preprocessed with in-house software LilaX and Medeia (provided by Gerhard Bracic). Signal intensity was quantified as the peak-to-peak height of the first derivative of the absorption spectrum. The CM radical (nitroxyl radical) intensity was converted to concentration using the stable nitroxyl radical of 100 μM Tempol (4-hydroxy-2,2,6,6-tetramethylpiperidine 1-oxyl) as a reference standard. Due to the variable number of available isolated MCs from preparations, different numbers of cells (approx. 3.5 to 6 $\cdot 10^5$) were used for individual experimental series. For presentation and calculation of means and standard deviation, signal intensities were normalized to 0.5 Mio cells, if not stated otherwise. The signal height of the oxygen-dependent saturation of the trityl signal was analyzed to determine oxygen consumption [31]. As a control, all experiments were run in reference to unstimulated cells. In addition, all combinations of added substances were tested for unwanted signal production by CMH to exclude artefacts.

2.6. Fluorescence-based ROS measurements

Extracellular H_2O_2 production by MCs was measured using the H_2O_2-sensitive and H_2O_2-specific fluorescent dye Amplex UltraRed (AUR) (Invitrogen, Molecular Probes, A36006), following the manufacturer's instructions. Assay component concentrations were 50 μM for AUR, 0.5 U/ml for horseradish peroxidase, and 100 U/ml for superoxide dismutase (SOD) (for sufficient conversion of $O_2^{\bullet -}$ to H_2O_2). H_2O_2 production was triggered by Tg and PMA (1 μM). Experiments were performed in 96-well plates (black/transparent) using the Tecan GENios Pro Reader with a bottom reading setting. All experiments were conducted in Ringer solution (1 mM Ca^{2+}) with 25,000 cells per well as duplicates or triplicates. [H_2O_2] was calculated from relative fluorescence units (RFU) after calibration of the system.

2.7. Voltammetry and UV/Vis photometry

Voltammetric measurements were performed with an Autolab Potentiostat/Galvanostat (PGSTAT 12, Metrohm, Netherlands) controlled by GPES 4.9 software. All data were recorded at 22 ± 1°C in unstirred solution using a three-electrode configuration in a one-compartment cell. Either a glassy-carbon (GCE) or a platinum (Pt) electrode (∅ 2 mm) was used as working electrode, while saturated silver/silver chloride (Ag/AgCl (3 M KCl)) and platinum wire served as a reference and counter electrode, respectively. Before each experiment, the working electrode was polished with 0.3 μm alumina powder, sonicated in distilled water and ethanol for 30 s, then rinsed with water and ethanol, and dried in air.

UV/Vis spectra were recorded with an Ultrospec™ 2100 *pro* spectrophotometer with a xenon lamp as a light source. The instrument was controlled by SWIFT II-LAB Applications Software (GE Healthcare Life Sciences/Biochrom Ltd, England). Spectra were measured at 22 °C between 200 and 350 nm wavelengths with a resolution of 1 nm.

For both methods, samples were freshly prepared and immediately measured within 1–3 min. UV/Vis control spectra recorded at later time intervals up to 90 min did not show any further spectral changes (see Suppl. Fig. 6).

2.8. Data analysis and statistics

Data of the different experiments were subsequently processed, visualized, and fitted with OriginPro 2019 or 2022 (OriginLab). Chemical structures were sketched with Accelrys Draw 4.1 (Accelrys Inc.). For visualization and energy minimization of the 3D structures, the software tools WebLab Viewer, Avogadro, and Discovery Studio 1.6 (Accelrys) were used.

The evolution of the ESR signal of the CM radical as a measure of superoxide formation in PMA-stimulated MCs was evaluated by averaging the time courses of each experiment for all donors (n = 14) to obtain the mean and standard deviation (SD). The mean curve and the +SD and -SD curves were constructed and displayed to show the variability of the cell experiments. The first 3 min (4 data points in the linear regime) of the three curves were used to define the mean kinetic rate and its SD. This result was displayed as a reference point in the 2-APB inhibition experiments after PMA stimulation. The same procedure was also applied for experiments on thapsigargin- and ionomycin-stimulated MCs. For evaluation of ratiometric Fura-2 imaging experiments, signals of cells (>100) were averaged and displayed as mean and ±SEM (standard error of mean).

3. Results

3.1. 2-APB suppresses NOX2-induced superoxide in a Ca^{2+}-independent way

The primary ROS released into extracellular space upon activation of

NOX2 in human MCs is the radical species $O_2^{\bullet -}$ which was monitored using the cell-permeable, superoxide-sensitive spin probe CMH. This cyclic hydroxylamine rapidly transfers one electron to $O_2^{\bullet -}$ forming hydrogen peroxide and a CM nitroxide radical ($CM^{\bullet}$), which is inert towards H_2O_2 and rather stable against bioreduction (Suppl. Fig. 1a, left panel) [32,33]. Thus, formation of $CM^{\bullet}$ as recorded by electron spin resonance (ESR) spectroscopy is a quantitative measure of superoxide production. The detection of superoxide was confirmed by suppression of the $CM^{\bullet}$ ESR signal by superoxide dismutase (Suppl. Fig. 1a, right panel).

Superoxide production in MCs was stimulated by the SERCA inhibitor Tg which induces SOCE in the presence of extracellular Ca^{2+} (Fig. 1a, dashed blue line) [34]. Applying 2-APB suppressed superoxide production below background production of unstimulated cells (Fig. 1a, solid blue line, and black line), probably by inhibiting SOCE and subsequent activation of NOX2. In absence of extracellular Ca^{2+}, Tg was not able to induce ROS production [29]. Ionomycin-induced ROS production was also inhibited by 2-APB (Fig. 1a, cyan lines). Ionomycin raises Ca^{2+} itself as a Ca^{2+} ionophore but also indirectly through SOCE activation [10]. Considering that 2-APB completely inhibits superoxide production below background production with both Tg and ionomycin, it appears likely that 2-APB not only interferes with SOCE but also with another process leading to superoxide production. To test this hypothesis directly, we used the phorbol ester PMA (phorbol-12-myristate-13-acetate) which activates phosphokinases PKC stimulating NOX2 independently of cytosolic Ca^{2+} as the absence of extracellular Ca^{2+} did not change ROS production (Suppl. Fig. 1a right panel, see also ref [29]).

Fig. 1b (upper panel) shows that 2-APB inhibits ROS production also under these Ca^{2+}-independent conditions in a dose dependent manner as inferred from the decreasing initial slopes of the $CM^{\bullet}$ production curves (during the first 3 min). Furthermore, the saturation levels at the end of the measurements dropped in correlation with 2-APB concentrations. Thus, 2-APB must inhibit NOX-induced superoxide production independent on available Ca^{2+}.

Because oxygen was fully consumed in presence of up to 50 μM 2-APB as simultaneously monitored by the trityl radical signal (Fig. 1b, lower panel) indicating NOX2 activity, the smaller final $CM^{\bullet}$ concentrations are not explained by reduced NOX2 activity. This result rather suggested a competitive reaction of 2-APB with superoxide, which then was no longer available for oxidation of CMH, thus decrementing $CM^{\bullet}$ formation. When applying 100 μM 2-APB, superoxide formation and oxygen consumption were completely abolished showing that enzymatic activity was hindered (Fig. 1b). Consequently, 2-APB exhibited a twofold effect: (i) an inhibition of NOX2 activity as read off from the initial slopes and (ii) a direct interaction with H_2O_2 and/or its radical precursor $O_2^{\bullet -}$ as inferred from decreased saturation levels at full oxygen consumption. Normalized dose-dependencies of NOX2 inhibition were similar when comparing initial production rates of the primary ROS superoxide from ESR (Fig. 1d, blue diamonds and fit curve) and hydrogen peroxide formed by dismutation of $O_2^{\bullet -}$ as measured by the Amplex UltraRed assay for PMA-stimulated MC of the same preparation batch (Fig. 1d, red dots and fit curve).

It should be noted that the response of primary human MCs to PMA stimulation is strongly depending on the human donor. A large variability of superoxide ($CM^{\bullet}$) formation was observed as indicated by the mean curve and the two curves derived from the experimental (n = 14) standard deviation in Fig. 1c. This variability is also observed in Fig. 1d for the mean slope (violet square) and its SD in absence of 2-APB. Analysis of further inhibition experiments of PMA stimulated MCs (n = 3) showed a likewise large variation of half inhibition values as low as 0.87 ± 0.25 μM/s and an intermediate value around 6.42 ± 1.6 μM/s (Suppl. Fig. 1b and c). In addition, such a pronounced variability in superoxide production was also observed for Tg and ionomycin

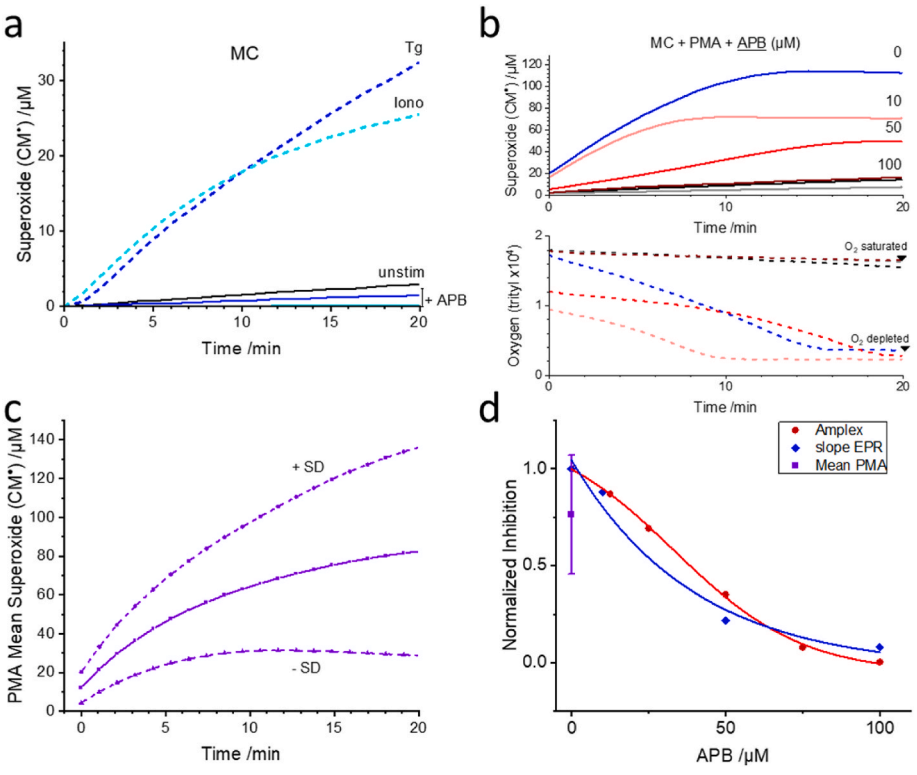

Fig. 1. 2-APB suppresses NOX2-mediated superoxide production of primary human monocytes. (a) Superoxide production was quantified by ESR using the spin probe CMH. MCs were stimulated (dashed lines) using 1 μM thapsigargin (Tg, blue trace) or 2 μM ionomycin (Iono, cyan trace); for cells exposed to 50 μM 2-APB, the ESR signal was suppressed (solid lines) below the black line of untreated monocytes. (b, top) Ca^{2+}-independent superoxide production stimulated with 1 μM PMA was suppressed by increasing 2-APB concentrations in an exemplified experiment, black line represents unstimulated MC and grey line unstimulated MC with 50 μM 2-APB; (b, bottom) simultaneous oxygen consumption measured from the ESR signal intensity changes of the trityl radical, levels for saturated and depleted state are indicated by triangles. (c) Variability of PMA-stimulated $O_2^{\bullet -}$ production with the mean response curve (solid violet trace) and ±SD curves (dashed) from n = 14 independent experiments of 14 blood donors. The slopes of the mean and the ±SD curves for the first 3 min were translated to the normalized mean point with SD bars in panel (d), violet point. (d) Normalized dose-response curves of 2-APB inhibition on superoxide production as measured by ESR from panel b (top) and H_2O_2 formation from the same sample batch by the Amplex UltraRed assay. The curves were fitted by a mono-exponential function for $O_2^{\bullet -}$ (blue trace) and Boltzmann function for the Amplex H_2O_2 assay (red trace). They gave comparable values for half inhibition of 28.3 ± 15.4 and 33.18 ± 3.01 μM with adj. R^2-values of 0.947 and 0.998, respectively. (For interpretation of the references to color in this figure legend, the reader is referred to the Web version of this article.)

stimulation (Suppl. Fig. 1d and e) for which inhibition by 2-APB was not systematically examined. However, in all cases (n = 8) a nearly complete suppression of ROS production was observed after addition of 50 μM 2-APB.

3.2. Quantification of 2-APB hydrolysis

In their explorative study on 2-APB and several analogues, Hofer et al. observed hydrolysis of 2-aminoethyl borinic esters when trying to purify 2-APB and derivatives by preparative RP-HPLC or column chromatography [21]. They also showed that 80% of chloroform-dissolved 2-APB hydrolyses to diphenylborinic acid (DPBAc) and 2-aminoethanol (2-AE), when exposed to water. To quantify the degree of hydrolysis, which likely also occurs in physiological experiments, and to understand possible reactions of 2-APB and its hydrolysis products with H_2O_2, we first needed to analyze its behavior in aqueous environment in more detail. ^{1}H NMR analysis of 2-APB in DMSO-d_6, the common solvent for 2-APB stock solutions, showed a signal pattern which was indicative for a cyclic conformation of the molecule, exclusively present in aprotic solvents, due to the amino protons observed around 6 ppm (see Suppl. Fig. 2a) [16]. Conversely, when 2-APB was dissolved in an aqueous solution, additional signals were found next to residual resonances of 2-APB (Suppl. Fig. 2b), which were identified with diffusion-ordered spectroscopy (DOSY) clearly showing that the peaks below 4 ppm shift derive from free 2-aminoethanol (Suppl. Fig. 2c). As expected, DOSY spectra of 2-APB in DMSO-d_6 showed only one molecule, i.e., intact 2-APB (Suppl. Fig. 3a). Moreover, spiking of 2-APB in deuterated phosphate buffer with pure 2-AE and DPBAc (spectra in Suppl. Fig. 3b) clearly showed in ^{1}H NMR that aqueous solutions of 2-APB mainly consist of DPBAc and 2-AE (Suppl. Fig. 3c). Less than 10% intact 2-APB was found under these conditions (10 mM 2-APB and 10% v/v DMSO-d_6). Likewise, we could observe partial re-esterification when spiking this solution with an equimolar amount of 2-AE (10 mM). Then, the portion of the well resolved resonances assigned to residual 2-APB (marked with * in Suppl. Fig. 3c) increased about twofold from 9.8% to 17.5% whereas the DPBAc lines at 7.55 ppm (Suppl. Fig. 3b) dropped from 90.2% to 82.5%. Under these conditions 2-APB was quite unstable and hydrolyzing to an equilibrium distribution favoring DPBAc over 2-APB (insert in Fig. 2) in agreement with findings by Hofer et al. [21] and Gao et al. [23].

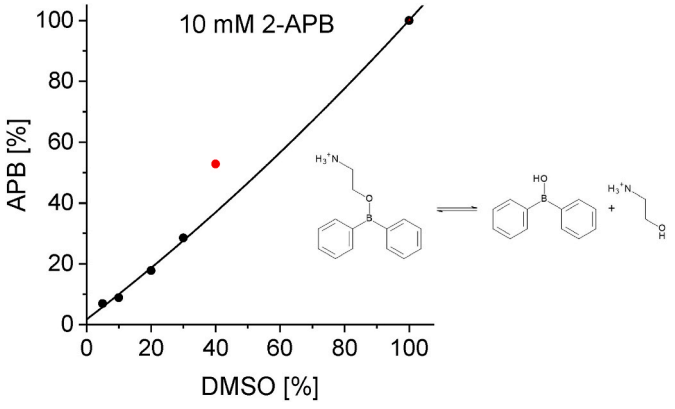

Fig. 2. 2-APB hydrolysis depends on DMSO content. Residual 2-APB concentration percentages were obtained from comparing integrals of resolved 2-APB and 2-AE ^{1}H NMR resonances (3.97 and 3.80 ppm, respectively) in the DMSO-d_6/D_2O mixtures (v/v) and in 100% DMSO-d_6. The data point for 40% DMSO content was not included in the fit due to incomplete miscibility and precipitation. The parameters of optimal linear-quadratic fit $y = y_o + a\,x + b\,x^2$ were $y_o = 1.706 \pm 1.548$, $a = 0.812 \pm 0.106$, $b = 0.00171 \pm 9.458E\text{-}4$ with $R^2 = 0.99933$ showing a small quadratic contribution and a range of residual 2-APB from 0.158% to 3.254% for a 10 mM 2-APB input and 0.1% DMSO in the solution. The insert shows the hydrolysis products 2-AE and DPBAc.

Because we expected that DMSO content in an aqueous solution is shifting the 2-APB hydrolysis equilibrium, the ^{1}H NMR spectra for 10 mM 2-APB in pure DMSO-d_6 and in 5–40% v/v mixtures with deuterated phosphate buffer were measured. The residual amount of 2-APB was estimated from integrals of resolved resonances assigned to 2-APB in the mixtures compared to pure DMSO. The range between 40% and 90% DMSO content could not be evaluated due to problems with miscibility and precipitation. As shown in Fig. 2, the 2-APB concentration drops drastically with decreasing DMSO content, which can be optimally fitted with a linear-quadratic function. With this curve we can interpolate to very low DMSO concentrations (0.1%) used in physiological experiments which gives about 1.8% of residual 2-APB, initially solved in DMSO. In a next step, typical physiological 2-APB concentrations of 50 μM were measured for various DMSO contents. Only for the 30% mixture we obtained sufficient 2-APB signals for quantification yielding only 0.55% as compared to 28.5% for 10 mM 2-APB input. Taking this scaling factor for the corresponding 2-APB concentrations, we arrive at a residual concentration of 17 nM for a 50 μM 2-APB input in 0.1% DMSO (with an error of ±14.9 nM as derived from the curve fit in Fig. 2).

Taken all together, our findings indicate that under physiological conditions 2-APB is nearly completely hydrolyzed, with DPBAc and 2-AE being the prevailing species. Our findings thus imply that studies that make use of 2-APB as an inhibitor of SOCE but also as an H_2O_2 scavenger need to consider the degree of hydrolysis in each solvent as well as the exact experimental conditions.

3.3. 2-APB reacts with hydrogen peroxide forming a new product

The hypothesis of a potential direct reaction of 2-APB with ROS was tested by monitoring breakdown of H_2O_2 in presence of increasing 2-APB concentrations. With the hydrogen peroxide specific Amplex UltraRed assay an exponential decay of H_2O_2 was obtained (Fig. 3a). Because several reactive species (H_2O_2, Amplex fluorochrome and its radicals, 2-APB, and reaction products) may interfere in this assay, direct reaction of 2-APB and H_2O_2 was checked with square-wave voltammetry (SWV) as an additional and independent method. First, the electrocatalytic oxidation of H_2O_2 to O_2 was studied on a platinum electrode (Fig. 3b). The peak current of H_2O_2 (at $E = 0.270$ V) decreased with increasing 2-APB concentration, while another peak associated to a new redox active product arose at $E = 0.535$ V. In the inverse experiment, transformation of 2-APB to a new product in presence of different H_2O_2 concentrations was followed on a glassy-carbon electrode (Fig. 3c). Here, the new peak was observed at a similar potential, around 0.510 V, whereas H_2O_2 was not detectable. Performing the analogous experiment with UV/Vis spectroscopy further showed the formation of a reaction product with increasing H_2O_2 concentrations (Fig. 3d). These three different experimental approaches clearly showed that 2-APB reacted with H_2O_2 producing a new product, and it appeared that 2-APB was completely decomposed by equimolar H_2O_2 concentrations. However, the observed changes in the SW peak current and absorption intensities in UV/Vis spectra for non-equimolar conditions were indicative of intermediate reactions and products. Moreover, shifting of the redox peak suggested a change in the local pH and involvement of protons in the redox reaction at the electrodes.

3.4. Identification of reaction products with H_2O_2

The near-to-complete decomposition of 2-APB to DPBAc and 2-AE implies that its reaction with H_2O_2 should mainly concern the hydrolysis products. To explore the reaction mechanism, 2-APB dissolved in aqueous buffered solutions was treated with increasing H_2O_2 concentrations and products were analyzed with ^{1}H NMR. The spectral changes for various selected ratios of 2-APB:H_2O_2 input are shown in Fig. 4a. The trace 1:0 highlights the pronounced hydrolysis of 2-APB (residual 2-APB marked by asterisks) to DPBAc (>7.1 ppm) and 2-AE (<3.9 ppm). With increasing the relative H_2O_2 portion, DPBAc and 2-APB signals were

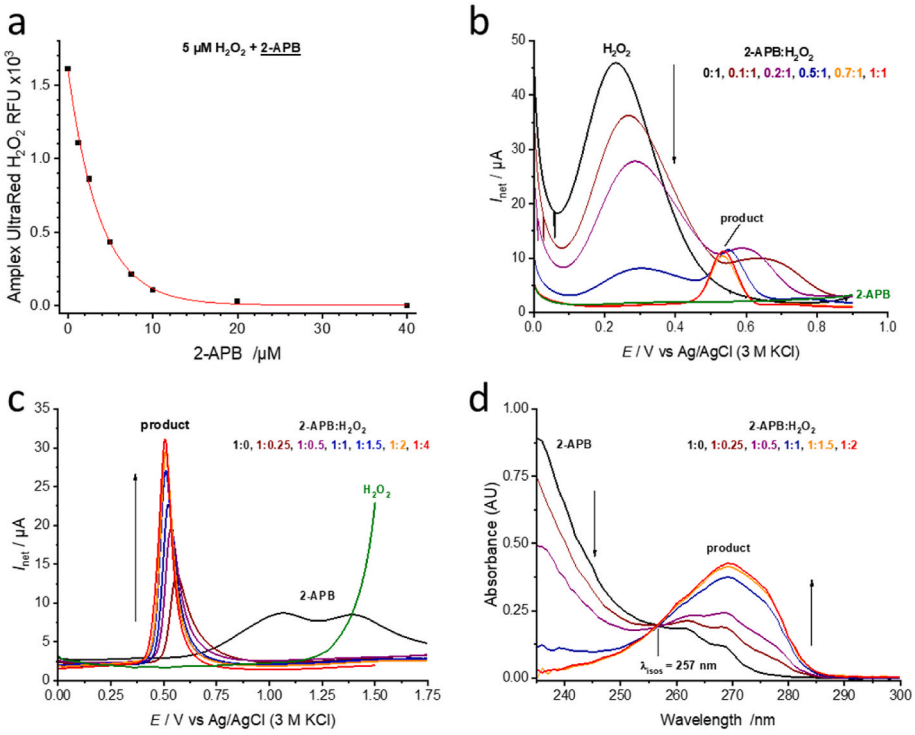

Fig. 3. 2-APB reacts with H_2O_2. (a) Consumption of 5 µM H_2O_2 by 2-APB was monitored using the fluorescence-based assay (Amplex UltraRed, HRP), data were fitted with a mono-exponential decay function. (b) Electrochemical detection of H_2O_2 on a platinum electrode, 10 mM H_2O_2 was exposed to increasing 2-APB concentration given as 2-APB: H_2O_2 ratios; the green curve is obtained for 2-APB in absence of H_2O_2. (c) shows the electrochemical response of 10 mM 2-APB on a glassy carbon electrode with increasing H_2O_2 given as ratios, the green curve is measured for 10 mM H_2O_2 alone. (d) UV/Vis spectral changes of 200 µM 2-APB with increasing H_2O_2 concentrations given as ratios. Samples were immediately measured within 1–3 min. Experimental conditions were for (b) and (c) 0.2 M potassium phosphate buffer (KPB) with pH 7.6, 5% v/v DMSO, $E_{sw} = 50$ mV, $\Delta E = 1$ mV, $f = 10$ Hz (b) or 50 Hz (c), and (d) 0.2 M KPB, 1% v/v DMSO. All experiments were performed at room temperature. (For interpretation of the references to color in this figure legend, the reader is referred to the Web version of this article.)

decaying and were completely consumed at equimolar H_2O_2 concentrations (trace 1:1). Concomitantly, two groups of new lines associated to products appeared, which had equal signal intensities as measured by the integrals. Further increase of H_2O_2 content led to gradual loss of product 1, while product 2 was gaining intensity. For a 1:2 ratio, product 2 was the remaining compound together with 2-AE. The quantitative behavior of the reaction is compiled in Fig. 4b. While 2-APB and DPBAc were vanishing for 1:1 ratio, 2-AE was slightly increasing probably due to additional release from decay of residual 2-APB but otherwise was not affected by H_2O_2 even for a four-fold H_2O_2 excess. Further details of reaction of 2-APB with H_2O_2 could not be resolved due to the low concentration of residual 2-APB. Both products increased in their relative concentrations up to 1:1 ratio (Fig. 4c). For higher 2-APB:H_2O_2 ratios, product 2 gained on expense of product 1 for ratios up to 1:2 and then stayed unaffected for up to 4-fold excess of H_2O_2.

Identification of both products was accomplished by spiking the equimolar mixture of 2-APB and H_2O_2 with 2-AE, DPBAc, phenylboronic acid (PBAc) and phenol (Ph). In the left panel of Fig. 5 the bottom spectrum shows the aromatic ring proton region of the mixture. Addition of 2-AE increased only the resonances of unbound 2-AE below 3.9 ppm shift (Suppl. Fig. 3c). When DPBAc was added to the 1:1-reacted solution, three additional groups of major lines were present located at identical shifts as obtained from pure DPBAc (Fig. 5, red spectra). The observation confirmed the complete decay of DPBAc in presence of equimolar H_2O_2 as shown in Fig. 4b. Adding the possible decay product PBAc to the 1:1 solution led to a signal increase of resonances assigned to product 1 with the identical line pattern measured for PBAc alone (Fig. 5, blue spectra). This finding proved that PBAc corresponds to product 1. In the same way, product 2 was identified as Ph from enhancing the associated resonances as shown in Fig. 5 (green spectra). The results clearly showed that the hydrolysis product of 2-APB, DPBAc, was not stable in presence of equimolar H_2O_2 and decomposed to PBAc and Ph. Additionally, it agreed well with the H_2O_2 titration NMR experiments for 1:2 and higher ratios (2-APB:H_2O_2) clearly giving the line pattern of Ph as the final product for H_2O_2 excess (Fig. 4a, c). In this context, it is also noted that DPBAc may also not be completely stable in aqueous solution, even in absence of H_2O_2, since minor resonances compatible with PBAc were detectable in the spectrum of pure DPBAc (Fig. 5, lower red spectrum).

The decay of DPBAc, formed from 2-APB hydrolysis, in presence of H_2O_2 was also tracked by ^{11}B NMR in deuterated phosphate buffer. Spectra were calibrated to boric acid (BAc) and corrected for sample pH according to the known pH-dependent shifting of BAc [35] (for details see Suppl. Fig. 4). Boron signals of dissolved 2-APB and DPBAc were found in the region between −10 and −20 ppm with respect to BAc as shown in Fig. 5, right panel, for the lower three spectra.

Addition of not quite stoichiometric amounts of H_2O_2 to 2-APB gave two new ^{11}B signals around 0 ppm and +8 ppm, which were assigned to BAc and, as per ^{1}H NMR, to the compound PBAc, respectively (Fig. 5, right panel, 2nd from top). Due to the incomplete reaction, we could still observe a broad signal in the DPBAc shift region (−10 to −20 ppm). For a four-fold excess of H_2O_2, only the signal of BAc at 0 ppm shift was left indicating complete conversion of DPBAc to Ph and BAc. Similar to the observation in ^{1}H NMR spectra of DPBAc (Fig. 5, left panel), a small ^{11}B signal of PBAc is detected due to some obvious instability of DPBAc under these conditions. The resolved chemical changes of the hydrolysis product DPBAc in presence of H_2O_2 are summarized in Scheme 1. For sub- to stoichiometric concentrations of H_2O_2, PBAc and Ph are the prevailing products, of which PBAc is further decomposed to boric acid and phenol for increased H_2O_2. This last step was shown to occur stoichiometrically for a 1:1 ratio of PBAc: H_2O_2 [36,37]. The combination of ^{1}H and ^{11}B NMR thus clearly showed that 2-APB/DPBAc is completely decomposed to phenol and boric acid for H_2O_2 excess.

3.5. *H_2O_2-reacted 2-APB loses inhibitory activity on SOCE*

Initiated by natural or artificial stimuli, immune cells are generally activated by SOCE and can produce considerable amounts of ROS as a defense strategy [27–29,38]. In this context, 2-APB is often used as a pharmacological tool to study SOCE-dependent activation mechanisms, and it has originally been shown to inhibit I_{CRAC} in Jurkat T cells and RBL-1 cells [11,39]. In the light of our findings, we evaluated the effect of 2-APB exposed to H_2O_2 on SOCE in Jurkat T cells by monitoring cytosolic calcium using the ratiometric calcium sensor Fura-2 on a single

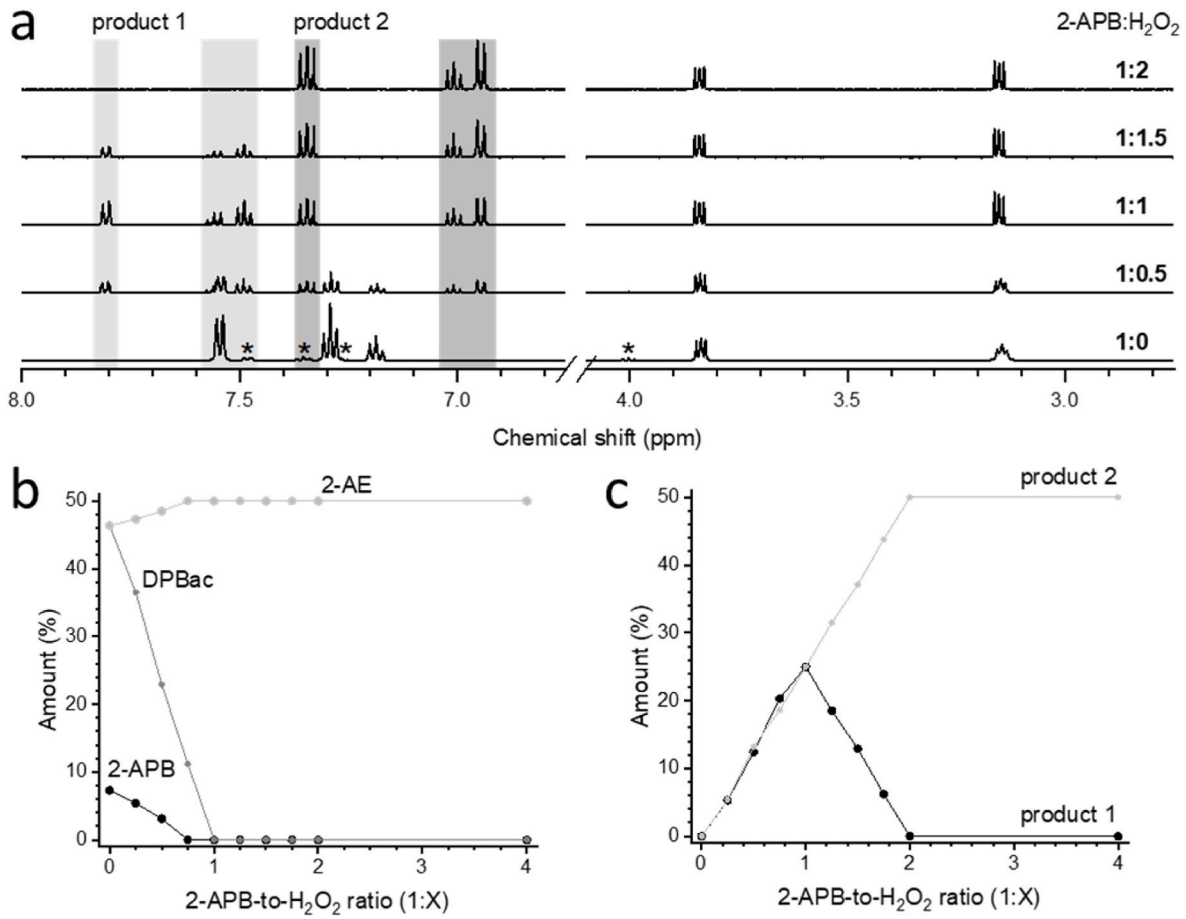

Fig. 4. Product formation from reaction of H_2O_2 with 2-APB/DPBAc. 10 mM 2-APB was dissolved in 0.2 M d-PB (5% DMSO-d_6) and increasing H_2O_2 concentrations (2.5–20 mM H_2O_2, i.e., 0.25-2-fold) were added to follow reaction and intermediate products. (a) ^{1}H NMR spectra of exemplary 2-APB/H_2O_2 reaction mixtures, given as ratios, are shown; in the spectrum of the 2-APB:H_2O_2 mixture 1:0, DPBAc and 2-AE are the major species while asterisks mark signals of residual 2-APB; correlated signals in the phenyl-proton region of products 1 and 2 are highlighted in light and dark grey, respectively. In (b) 2-APB and its hydrolysis products and (c) reaction products detectable by ^{1}H NMR are quantified for up to 4-fold excess of H_2O_2. The integrals of the following resonances were evaluated: 2-AE, t(2H) at 3.84 ppm; 2-APB, t(2H) at 4.0 ppm and d(4H) at 7.48 ppm or only t(2H) at 4.0 ppm, when H_2O_2 was present; DPBAc, t(4H) at 7.18/7.19 ppm; product 1, d(4H) at 7.81 ppm; product 2, t(2H) at 7.01 ppm or t(4H) at 7.35 ppm for $H_2O_2 \geq 0.75$-fold. Total intensity of detected reactants and products was set to 100%, sum of product (DPBAc + product 1 + product 2) was equalized to 2-AE. At $H_2O_2 \geq 0.75$-fold, 2-AE was set to 50% because 2-APB was no longer detectable and, hence, 50% 2-AE must have been present.

cell level. Tg was used for depletion of ER calcium stores and to induce subsequent SOCE, which is caused mainly (or potentially even exclusively) by CRAC channels in T cells including Jurkat T cells (reference [40] summarizes this in detail). To discriminate effects on extracellular calcium entry and intracellular calcium release, pure or H_2O_2-treated 2-APB was added after ER store depletion in absence of external calcium or after induction of SOCE. In agreement with many other reports [11,12,15,41], 50 μM 2-APB/DPBAc fully inhibited SOCE (Fig. 6a and b, red line), whereas a small residual SOCE activation was seen for 25 μM 2-APB/DPBAc (Fig. 6a, orange trace). Adding 2-APB, which was reacted with a 1:2 2-APB:H_2O_2 ratio for complete decomposition of 2-APB and DPBAc to BAc and Ph (cf. Figs. 4c and 5 right panel and Scheme 1), completely abolished the inhibitory effect (Fig. 6b, dark cyan trace, and black lines for DMSO as vehicle). Hence, the final products, Ph and BAc, could not substitute the inhibitory effect of 2-APB/DPBAc. Equimolar mixtures of 2-APB and H_2O_2 resulted only in partial inhibition of SOCE (Fig. 6b, grey trace) even though 2-APB/DPBAc should be completely transformed to phenol and phenylboronic acid (cf. Fig. 4b and c).

Next, we tested the effect of 2-APB and its decomposition products in the presence of external calcium (0.5 mM Ca^{2+}, Fig. 6c). As expected, addition of 50 μM 2-APB/DPBAc (final DMSO 0.1%) disrupted calcium influx after Tg stimulation compared to DMSO vehicle alone (red vs. black trace). Likewise, 2-APB reacted with half equimolar H_2O_2 (1:0.5 ratio) showed the same inhibitory effect (blue trace). Adding the solution of 2-APB, reacted with twofold H_2O_2 excess (1:2 ratio) and consisting only of the final products Ph and BAc, completely abolished inhibition (Fig. 6d, dark cyan trace) compared to non-treated 2-APB (red trace). When an equimolar mixture was applied after activating SOCE, an additional calcium peak was observed (grey trace). This finding implied that the incomplete inhibition of SOCE in the re-addition protocol (Fig. 6b) was in fact due to calcium influx. Importantly, this influx was not caused by depletion of internal stores, since addition of the 1:1 mixture in absence of extracellular calcium did not result in an increase of cytosolic calcium (Fig. 6a and b, at 10 min). This external calcium influx could be inhibited applying 50 μM 2-APB and reactivated upon adding the 1:1 mixture again (Suppl. Fig. 5a). Moreover, SOCE activation by the intermediate reaction product phenylboronic acid (PBAc), added as a pure substance, was excluded in control experiments (Suppl. Fig. 5b). Two explanations for the activating effect of the 1:1 reaction mixture appeared possible: (i) Small errors in exact adjustment of equimolar concentrations could have left submicro- or micromolar concentrations of 2-APB/DPBAc. As inferred from the steep slope of DPBAc in the NMR H_2O_2 titration in d-PB (Fig. 4b) a remaining portion of 1% DPBAc was compatible with a 1–2% deviation from perfect equimolarity. (ii) The degradation reaction with H_2O_2 was depending on solvent and its pH. When changing the NMR solvent to D_2O/1 mM NaOD

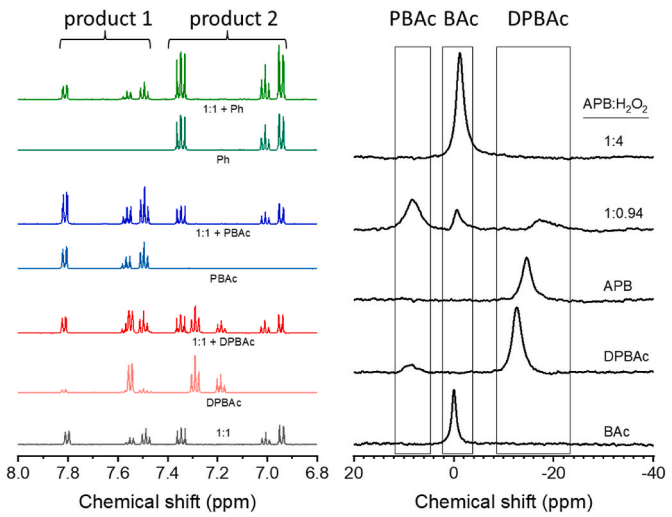

Fig. 5. Identification of reaction products of 2-APB/DPBAc with H_2O_2 by ^{1}H and ^{11}B NMR. Left panel ^{1}H NMR: For the 1:1 equimolar reaction of 10 mM 2-APB with 10 mM H_2O_2 in 0.2 M d-PB (10% DMSO-d_6), reaction products were identified by amplification of signal patterns by spiking with 20 mM phenol (Ph), 10 mM phenylboronic acid (PBAc), and 10 mM DPBAc; The diagram shows ^{1}H NMR spectra of the 1:1 reaction (bottom, black trace), the pure spiking substances, and the spiked reaction solution each stacked on top in pairs with similar colors. Right panel ^{11}B NMR: The boron resonances of 10 mM BAc (boric acid) in 0.2 M d-PB, 30 mM DPBAc and 30 mM 2-APB in 0.2 M d-PB (15% DMSO-d_6) correspond to the lower three spectra (as indicated on the right-hand side). The upper two spectra were obtained from the reaction of 30 mM 2-APB with H_2O_2 in 1:0.94 and 1:4 ratios. The resonance at +8 ppm shift is associated with PBAc. All spectra were calibrated to −0.05 ppm for boric acid. The rectangles highlight the assignment of resonances to the substances or reacted solutions. (For interpretation of the references to color in this figure legend, the reader is referred to the Web version of this article.)

(pH 11), we found 34% of residual DPBAc in the 1:1 reaction mixture (Suppl. Fig. 5c), clearly much more than in d-PB (Fig. 4b). Therefore, small deviations in pH and the different composition of the used Ringer buffer (vs d-PB) could also result in small micromolar 2-APB/DPBAc concentration remaining in the mix, which provoked the observed SOCE-activating effect of the 1:1 reaction mixture. Interestingly, concentrations of 2-APB (respectively DPBAc) lower than 10 μM were shown to activate SOCE in Jurkat T cells [11].

3.6. Effects of hydrolysis and degradation products of 2-APB on ROS formation

After establishing and quantifying the hydrolysis of 2-APB and the degradation of 2-APB/DPBAc by H_2O_2 we focused on applying the corresponding substances to stimulated ROS producing human MCs. To this end, the main hydrolysis product DPBAc, and the identified H_2O_2 degradation product PBAc (see Scheme 1) were added as pure substances to PMA-stimulated primary MCs. A typical data set (selected from several experiments of two blood donors) is shown in Fig. 7a. The phorbolester induced a steep rise of the $CM^{\bullet}$ ESR signal as a measure of $O_2^{\bullet-}$ which finally reached saturation after about 16 min (red trace). Upon addition of 50 μM and 100 μM 2-APB (blue solid and dashed traces, respectively), the signal build-up was progressively slowed down, and the saturation levels were reduced and reached at later time points (for 100 μM 2-APB not in the measurement window), which was also observed in Fig. 1. Qualitatively, a similar effect was obtained, when adding the same concentrations of DPBAc (green solid and dashed traces). In contrast, PBAc did not delay signal formation nor reduce saturation levels for both applied concentrations (orange solid and dashed curves), since they overlap with the curve for PMA stimulation. Control experiments with all added substances in absence of monocytes showed small signals at the background level (buffer, 1% DMSO, CMH and trityl, black trace in Fig. 7a) indicating that no redox reactions with CMH are impacting on the experiments.

As stimulated MCs produced large amounts of $O_2^{\bullet-}$, we simultaneously monitored oxygen consumption by intensity changes of the trityl radical signal to correlate both kinetics as shown in Fig. 7b. The time points of complete O_2 consumption were directly read from the intercept with the constant oxygen depletion level (indicated by the grey dotted line, which is associated with the minimal signal intensity of the trityl radical signal in absence of oxygen, Suppl. Fig. 1a, left panel) [31]. For PMA, PBAc and the 50 μM concentrations of 2-APB and DPBAc, the time points coincide with the transition of the superoxide ($CM^{\bullet}$) signal to the plateau in Fig. 7a. For the 100 μM concentration of 2-APB and pure DPBAc (dashed blue and green curve), the intercept with the oxygen depletion level is estimated with 119.5 min and 55.8 min, respectively, from a linear interpolation of the last 5 min for both curves. The time points for complete O_2 consumption are given in graph (b) with an estimated error of ±1 min. Here, we again observe a decrease in the initial ROS production rate with increasing 2-APB or DPBAc concentrations and a full consumption of oxygen as in Fig. 1. This implies that the kinetics of $O_2^{\bullet-}$ formation by NOX2 is considerably inhibited upon adding 2-APB or DPBAc. Although dissolved oxygen (approx. 200 μM in the glass capillary) is consumed, the saturation level of PMA stimulation without 2-APB or DPBAc is not reached which means that a portion of $O_2^{\bullet-}$ is escaping detection by CMH under otherwise identical conditions. It appears that 2-APB/DPBAc competitively scavenge $O_2^{\bullet-}$ and further decay to products which are not necessarily identical to H_2O_2 degradation products.

Although observing a variable response for PMA stimulation, we compared the ROS experiments of Figs. 7 and 1, which basically indicated a similar overall behavior using the identical method but different cell numbers ($2\bullet10^5$ vs $4.5\bullet10^5$ cells). The sigmoidal $CM^{\bullet}$ production curves for PMA-stimulated MCs in Fig. 7a showed a slope in the linear range (6–10 min) of 0.11 μM/s close to the mean of 0.127 μM/s determined from Fig. 1 and Suppl. Fig. 1. In addition, the time points for total O_2 consumption (19.3 min vs 16 min) were similar for both cell concentrations. Hence, the kinetics of $CM^{\bullet}$ formation was in the expected range in both cases. However, the saturation level for $CM^{\bullet}$ as a measure for total superoxide production were 80 μM $CM^{\bullet}$ (Fig. 7a, red curve) vs 110 μM $CM^{\bullet}$ (Fig. 1b top, blue curve) and did not scale linearly with the used cell number. For a more than twofold larger cell number, one would expect a saturation level around 160 μM $CM^{\bullet}$ for PMA stimulation which is even above the curve for + SD in Fig. 1c. Likewise, the incomplete inhibition even upon addition of 100 μM 2-APB/DPBAc in the experiment with lower cell number (Fig. 7a and b) gave prolonged oxygen consumption times but no full inhibition as seen in Fig. 1b. In conclusion, these unexpected differences in the inhibitory efficiency of 2-APB in the experiments of Figs. 1 and 7 are likely related to changed redox and antioxidant properties of the experimental system depending on cell density.

4. Discussion

Our NMR findings clearly show that 2-APB is stable only in pure DMSO and hydrolyzes with increasing water content (see Fig. 2) on a time scale below 1–2 min as derived from our different experimental approaches (Suppl. Fig. 6a). Quantitatively, for a 10 mM input of 2-APB in 0.1% DMSO/water about 98% are hydrolyzed to diphenylborinic acid (DPBAc) and aminoethanol (2-AE). In a typical physiological experiment with 50 μM 2-APB in 0.1% DMSO/buffer mixture we must assume a nearly complete conversion to DPBAc. Since DPBAc is a monoprotic acid, a pK_a value of 6.6 is calculated [42], which implies that, at a physiological pH 7.4, only about 17% of the hydrolysis product DPBAc are left in its protonated form. This neutral species (and remainder of 2-APB) can diffuse into or through the plasma membrane and may therefore interact with potential binding sites of the STIM-Orai

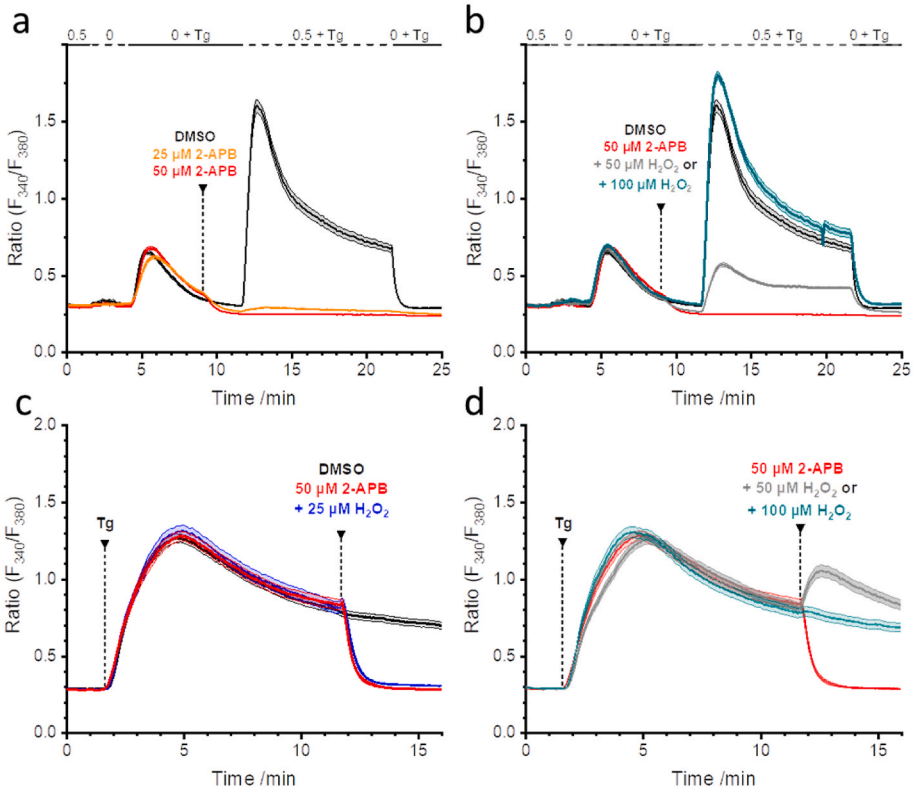

Fig. 6. Effect of 2-APB/H_2O_2 mixtures on store-operated calcium entry. Jurkat T cells were loaded with Fura-2 and imaged in modified Ringer buffer with different Ca^{2+} concentrations. Intracellular Ca^{2+} is given as ratio F_{340}/F_{380}. ER stores were depleted upon inhibition of SERCA with 1 µM Tg. 2-APB, the vehicle (DMSO, 0.1%) or a freshly prepared solution of 2-APB reacted with hydrogen peroxide was applied at indicated times. (a, b) Calcium re-addition protocol: in absence of calcium, stores were depleted, and 2-APB or reaction mixture was applied. SOCE was induced by adding 0.5 mM external Ca^{2+}. Ca^{2+} influx was fully suppressed by 50 µM 2-APB while some residual influx prevailed for 25 µM 2-APB (a, red and orange traces). In (b) influx was not suppressed for 2-APB reacted with double molar H_2O_2 (1:2 ratio 2-APB: H_2O_2, dark cyan trace); for an equimolar reaction with H_2O_2 a partial influx was observed (grey trace). (c, d) global calcium protocol: in 0.5 mM Ca^{2+} solution stores were depleted and SOCE activated, after 12 min 2-APB or reaction mixture was applied. In panel (c) 50 µM 2-APB and its solution reacted with half equimolar H_2O_2 (1:0.5 ratio) equally suppressed Ca^{2+} influx (red and blue trace). In (d) suppression of influx was completely abolished for a 1:2 2-APB:H_2O_2 solution (dark cyan trace) vs unreacted 2-APB (red trace). For the equimolar reaction 2-APB:H_2O_2 an activation was observed (grey trace). For evaluation, between n = 106 to 220 cells were averaged; the standard error of the mean (SEM) for each curve is shown as a colored band. Graphs a and b represent one experiment with all conditions measured on a single day. For c and d one out of three independent experiments is shown with conditions performed on one day. Cells were taken from the same preparation of the Jurkat T cell line. (For interpretation of the references to color in this figure legend, the reader is referred to the Web version of this article.)

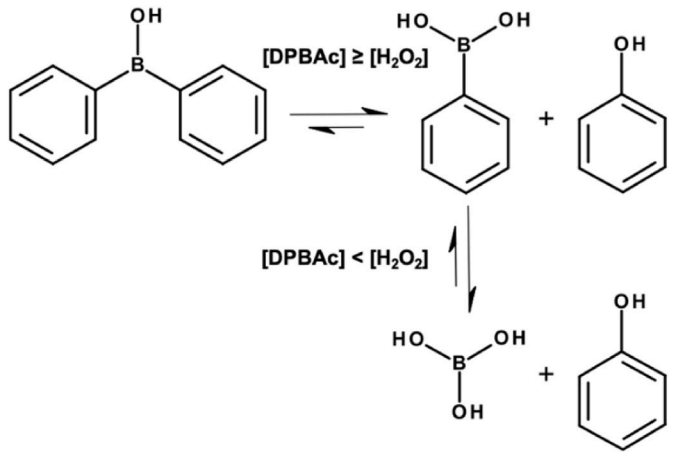

Scheme 1. Decomposition of diphenylborinic acid (DPBAc) by variable amounts of H_2O_2 in deuterated phosphate buffer.

complexes within the membranes or on the cytosolic side. In contrast, the negatively charged DPBAc should be confined to the extracellular space, where it could interact only with exposed outer loop components of the Orai complexes. A further possible intracellular species is related to re-esterification of DPBAc in presence of free 2-AE as observed in this study and by Hofer et al. in DMSO solutions with very slow kinetics (up to 48 h) [21]. In the context of working with cells, one should consider that cells may contain a pool of free 2-AE depending on its import into cells and the activity of postulated ethanolamine cycle based on degradation of phosphatidylethanolamine by phospholipases and rebuilding the phospholipid [43]. This pool may additionally be supplemented by diffusible 2-AE from 2-APB hydrolysis and could contribute to regaining 2-APB from its hydrolysis product DPBAc to some extent, despite a rather low association constant (4 M^{-1}) [44], and should occur preferentially in an aprotic environment.

It becomes evident for physiological experiments with 2-APB that one must consider the equilibrium of three species, remaining or re-esterified 2-APB, and protonated and deprotonated DPBAc, even with an asymmetric distribution between extracellular space and cell compartments. The major species should be the deprotonated and protonated DPBAc, for which a more pronounced SOCE inhibition (9.8 µM vs 22.9 µM for 2-APB) was found in HEK293 cells [21]. In this context it is noted, that the recently synthesized bis-boron compounds DPB162-AE and DPB163-AE both differentially inhibit (and DPB163-AE also activates) SOCE at a 50- to 100-fold lower IC50 in several cell types, which appears to be mediated by STIM [18,19]. When applied, they also carry aminoethanol groups, which, in the light of the presented findings, should also hydrolyze in aqueous buffers and may form protonated, deprotonated and possibly mixed bis-borinate compounds. This change in physicochemical properties in comparison to 2-APB might affect their distribution and their structural features. Further studies on these compounds are needed to define their hydrolysis products.

Taken together, our results and the reports by Hofer et al. [21] and Gao et al. [23] suggest that 2-APB is only stable in DMSO and will be largely hydrolyzed under conditions of physiological cell experiments. Consequently, for determining IC50 (or EC50) of 2-APB for inhibiting or activating Ca^{2+} signals during SOCE, one must consider rapid hydrolysis to DPBAc in the aqueous environment and adaptation of an equilibrium of minor amounts of 2-APB and protonated and deprotonated DPBAc. This result may also be important for the structural search of the potential binding sites of various Ca^{2+} channels factoring in the altered

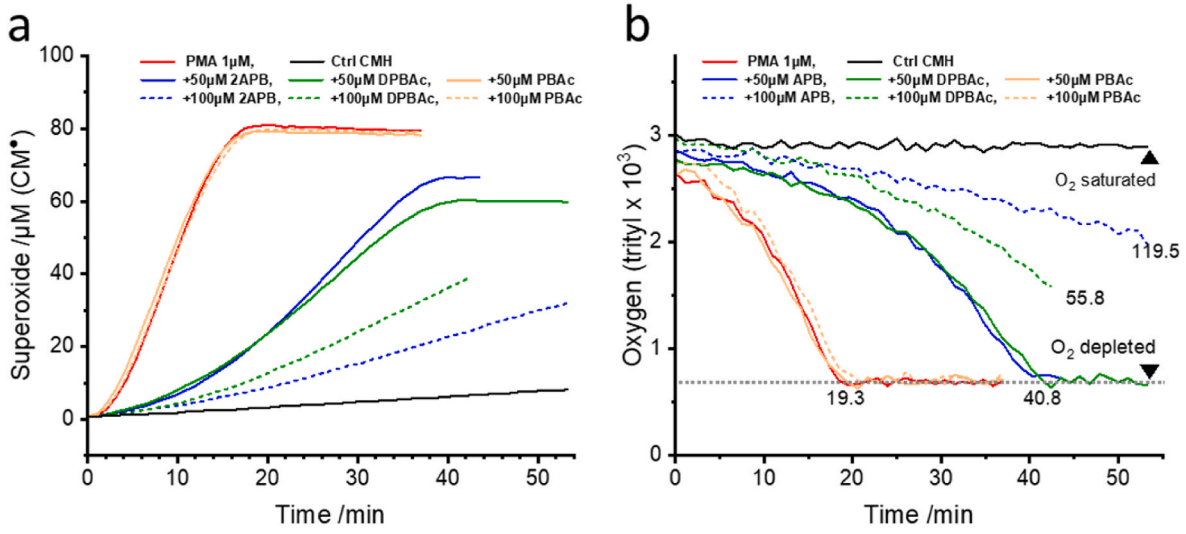

Fig. 7. Inhibitory and antioxidative effects of hydrolysis and degradation products of 2-APB. Primary MCs ($2x10^5$, representative experiment out of two from one donor) were stimulated with PMA (1 µM) and the ESR signals of $CM^•$ (a) and trityl (b) recorded. Relevant substances were added to PMA-stimulated MCs as indicated by the color code showing the corresponding change in superoxide formation (a) and oxygen consumption (b). The production rate for PMA-stimulated MCs in (a) was determined in the linear range (6–10 min) as 0.11 µM/s (±0.001 SEM). In (b) the horizontal grey dotted line indicates oxygen depletion level and the numbers the (interpolated) time points of O_2-depletion for each experiment. Results for the other donor and repetitive measurements qualitatively showed a similar behavior albeit with variable quantities as discussed for Fig. 1. Incubation time for boron compounds was approximately 2 min before first measurement. (For interpretation of the references to color in this figure legend, the reader is referred to the Web version of this article.)

structures and properties of the hydrolysis products.

A further aspect important for experiments with cells is the fact that the 2-APB hydrolysis product DPBAc is sensitive to $H_2O_2/O_2^{•-}$. It is rapidly reacting within about 1–5 min as derived from SW and UV/Vis experiments (Suppl. Fig. 6b) and degraded to phenylboronic acid (PBAc), phenol (Ph) and boric acid (BAc) depending on hydrogen peroxide concentration. This indicates that 2-APB/DPBAc are acting as strong antioxidants consuming two equivalents of H_2O_2 for complete conversion to Ph and BAc (Scheme 1). Interestingly, in a study exploring the cardioprotective effects of 2-APB in ischemia-reperfusion injury, the possible antioxidant properties were suggested to play a role in the pharmacological effects of 2-APB [45]. Cardiomyocytes pretreated with 2-APB were stressed with equimolar amounts of H_2O_2 but escaped inducible cell death due to the antioxidative effect. The authors also examined the chemical reaction of 2-APB with H_2O_2 by NMR and found as a final product phenol which was identified by thin-layer chromatography. The intermediate products, determined in our approach, were not accessible in their experiments using a ten-fold molar excess of H_2O_2 in the reaction solution.

The obvious instability of 2-APB/DPBAc towards hydrogen peroxide and the failure of degradation products to affect SOCE poses the question whether measurements of IC50 (or EC50) of 2-APB for inhibiting or activating Ca^{2+} channels may be modulated by the redox state of "resting" cells vs "stressed" cells and thus may result in different values. Clearly, in cell experiments with stimulated H_2O_2 production or an externally added H_2O_2 bolus the effective concentration and activity of simultaneously applied 2-APB/DPBAc will strongly depend on the molar ratios. This caveat was also invoked during ischemia-reperfusion experiments [45]. Thus, such data need to be interpreted with great care.

Our ROS experiments with PMA-stimulated MCs clearly show that 2-APB and its hydrolysis product DPBAc directly inhibit NOX2 activity and are concomitantly degraded in presence of ROS-forming cells. The final degradation products are completely incapable of inhibiting NOX2. The ESR data display a considerable variability depending on the human donor but also on the cell density. For the latter, we need to consider the redox properties of the complex cell system related to possible competing reaction pathways for the primary superoxide radical: (i) dismutation by SOD, (ii) spontaneous dismutation, (iii) reduction by CMH, (iv) reaction with components of the cell membrane and (v) scavenging by 2-APB or DPBAc (Suppl. Fig. 7). Reactions (ii), (iii) and (v) should be essentially independent on cell concentration and proceed unaffected with their inherent kinetic rate constants. In contrast, reaction (i) will be more probable for higher cell numbers. In this case, protonated superoxide diffuses more effectively to adjacent cells, where it will be rapidly dismutated by cytosolic SOD1. Subsequently produced H_2O_2, on the other hand, is degraded to oxygen and water by cytosolic catalase. Moreover, reaction (iv) may pose an additional sink for superoxide, because it is forming peroxyl-radicals ($R–OO^•$) on lipids and proteins which are degraded by cellular antioxidants in functional cells. This fraction of superoxide is thus escaping spontaneous dismutation (ii) and reduction by CMH (iii) to form $CM^•$ and H_2O_2 (see Suppl. Fig. 1). Consequently, for a significantly higher cell density one should not expect a proportional increase of $CM^•$ signal when compared to a much lower cell concentration. Conversely, for a low cell concentration as used in Fig. 7, less superoxide is degraded in proportion and might be responsible for a more effective scavenging by CMH and increased $CM^•$ and H_2O_2 yield. Furthermore, dismutation by SOD ((i) in Suppl. Fig. 7) and action of catalase should be less effective and together with reduced pathway (iv) might yield more H_2O_2 as a net effect. According to Scheme 1, the equilibrium would be shifted in favor of the non-inhibiting species PBAc, Ph and BAc. Consequently, less of inhibitory species 2-APB and DPBAc were available for partial or full inhibition of NOX2 in case of low cell density. This finding plus the inherent variability of samples from different donors is highlighting that experiments with primary human MCs must be interpreted carefully.

From our experiments with differently stimulated MCs, we deduce antioxidant properties and an additional inhibitory effect of 2-APB/DPBAc on NOX2 activity. At higher concentrations (>50 µM) formation of superoxide/hydrogen peroxide via NOX2 was strongly suppressed and concomitant oxygen consumption was reduced which was not achieved with the degradation products (PBAc, Ph). Diphenyleneiodonium (-chlorid, DPI) is a commonly used inhibitor for flavoproteins and particularly of the oxidative burst in stimulated neutrophils mediated by NOX2 [29,46,47]. It shares some essential structural features with 2-APB/DPBAc, two phenyl-groups and slightly exposed iodonium. As shown in Scheme 2, the diphenylene-group is planar

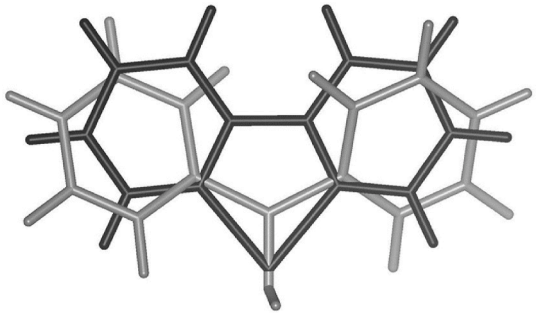

Scheme 2. Superposition of DPI (dark grey) and DPBAc (light grey) structures. The phenyl rings of DPBAc adopt an angle of ±15° versus the planar rings of DPI. Structures were minimized with Avogadro and Discovery Studio.

whereas in DPBAc the rings are slightly tilted by about 30° with respect to each other. There are, however, no gross deviations in the overall structure, even though the charges at the heteroatom should be different (iodonium: positively charged, boric group: neutral or negatively charged), but the flexibility of the phenyl rings in DPBAc can evidently be much larger. This differences are probably reflected by the quite different values for half inhibition of MC NOX2 by 2-APB/DPBAc (approx. 0.8–30 μM, see section 3.1) compared to about 0.5–2.5 μM for DPI [47]. The structural similarity of DPBAc and DPI points to a common binding motif, most probably the flavin-adenine dinucleotide (FAD) site, in NOX2 for both compounds.

In their ischemia-reperfusion study, Morihara et al. [45] observed reduced ROS levels and less inflammatory response by neutrophil infiltration following 2-APB treatment. Our findings indicate that, additionally, the inhibiting effect on NOX may contribute to a decrease of ROS production and support the cardioprotective effect.

5. Concluding remarks

2-APB does not only show versatile effects as a SOCE inhibitor and activator depending on its concentration (up to 100 μM) and channel type, but also exhibits a complex chemistry when present in aqueous cell systems. We confirmed and characterized the rapid hydrolysis of 2-APB in aqueous solutions and identified and quantified the prevailing species to be protonated and deprotonated diphenylborinic acid (DPBAc). Surprisingly, 2-APB/DPBAc showed a pronounced antioxidative effect reacting with superoxide or hydrogen peroxide. We found that 2-APB/DPBAc are degraded in a concentration dependent manner to phenol (Ph) and boric acid (BAc). Furthermore, we demonstrate that none of the products present in the reacted mixtures of DPBAc/H_2O_2 is affecting Ca^{2+} influx through SOCE or other types of channels. Similarly, the degradation products did not inhibit NOX2 whereas 2-APB/DPBAc completely suppressed the oxidative burst in activated monocytes. Both “new” 2-APB properties, i.e., antioxidant potential and inhibition of NOX2 enzyme, may have physiological and therapeutic relevance. The chemical instability and the presence of at least three active species need to be considered when studying the activation/inhibition of Ca^{2+} channels or when analyzing binding or interaction sites that modulate the store operated calcium entry (SOCE).

Funding

This project has been supported by the SFB 894 (project A1 to M.H.) and SFB1027 (project C4 to I.B.).

Declaration of competing interest

The authors declare that they have no known competing financial interests or personal relationships that could have appeared to influence the work reported in this paper.

Data availability

Data will be made available on request.

Acknowledgments

We very much appreciate the help of Prof. Hermann Eichler and the Institute of Clinical Hemostaseology and Transfusion Medicine at Saarland University Medical Center for obtaining human blood cells. We gratefully acknowledge Carmen Hässig for cell preparation. We also thank Gerhard Bracic for programming evaluation tools for ESR time series experiments, and Dalia Alansary and Barbara Niemeyer for support in Ca^{2+}-imaging experiments.

Appendix A. Supplementary data

Supplementary data to this article can be found online at https://doi.org/10.1016/j.redox.2023.102654.

References

[1] H.Z. Hu, J. Grandl, M. Bandell, M. Petrus, A. Patapoutian, Two amino acid residues determine 2-APB sensitivity of the ion channels TRPV3 and TRPV4, Proc. Natl. Acad. Sci. U.S.A. 106 (2009) 1626–1631, https://doi.org/10.1073/pnas.0812209106.

[2] H.Z. Hu, Q.H. Gu, C.B. Wang, C.K. Colton, J.S. Tang, M. Kinoshita-Kawada, L. Y. Lee, J.D. Wood, M.X. Zhu, 2-aminoethoxydiphenyl borate is a common activator of TRPV1, TRPV2, and TRPV3, J. Biol. Chem. 279 (2004) 35741–35748, https://doi.org/10.1074/jbc.M404164200.

[3] G. Kovacs, N. Montalbetti, A. Simonin, T. Danko, B. Balazs, A. Zsembery, M. A. Hediger, Inhibition of the human epithelial calcium channel TRPV6 by 2-aminoethoxydiphenyl borate (2-APB), Cell Calcium 52 (2012) 468–480, https://doi.org/10.1016/j.ceca.2012.08.005.

[4] J.P. Lievremont, G.S. Bird, J.W. Putney, Mechanism of inhibition of TRPC cation channels by 2-aminoethoxydiphenylborane, Mol. Pharmacol. 68 (2005) 758–762, https://doi.org/10.1124/mol.105.012856.

[5] D.E. Clapham, Calcium signaling, Cell 131 (2007) 1047–1058, https://doi.org/10.1016/j.cell.2007.11.028.

[6] R. Chokshi, P. Fruasaha, J.A. Kozak, 2-Aminoethyl diphenyl borinate (2-APB) inhibits TRPM7 channels through an intracellular acidification mechanism, Channels 6 (2012) 362–369, https://doi.org/10.4161/chan.21628.

[7] P. Malko, S.A. Syed Mortadza, J. McWilliam, L.H. Jiang, TRPM2 channel in microglia as a new player in neuroinflammation associated with a spectrum of central nervous system pathologies, Front. Pharmacol. 10 (2019) 239, https://doi.org/10.3389/fphar.2019.00239.

[8] T. Maruyama, T. Kanaji, S. Nakade, T. Kanno, K. Mikoshiba, 2APB, 2-aminoethoxydiphenyl borate, a membrane-penetrable modulator of Ins(1,4,5)P-3-induced Ca2+ release, J. Biochem. 122 (1997) 498–505, https://doi.org/10.1093/oxfordjournals.jbchem.a021780.

[9] H.T. Ma, R.L. Patterson, D.B. van Rossum, L. Birnbaumer, K. Mikoshiba, D.L. Gill, Requirement of the inositol trisphosphate receptor for activation of store-operated Ca2+ channels, Science 287 (2000) 1647–1651, https://doi.org/10.1126/science.287.5458.1647.

[10] M. Hoth, R. Penner, Depletion of intracellular calcium stores activates a calcium current in mast-cells, Nature 355 (1992) 353–356, https://doi.org/10.1038/355353a0.

[11] M. Prakriya, R.S. Lewis, Potentiation and inhibition of Ca2+ release-activated Ca2+ channels by 2-aminoethyldiphenyl borate (2-APB) occurs independently of IP3 receptors, J. Physiol.-London 536 (2001) 3–19, https://doi.org/10.1111/j.1469-7793.2001.t01-1-00003.x.

[12] C. Peinelt, A. Lis, A. Beck, A. Fleig, R. Penner, 2-Aminoethoxydiphenyl borate directly facilitates and indirectly inhibits STIM1-dependent gating of CRAC channels, J. Physiol. 586 (2008) 3061–3073, https://doi.org/10.1113/jphysiol.2008.151365.

[13] H.T. Ma, K. Venkatachalam, J.B. Parys, D.L. Gill, Modification of store-operated channel coupling and inositol trisphosphate receptor function by 2-aminoethoxydiphenyl borate in DT40 lymphocytes, J. Biol. Chem. 277 (2002) 6915–6922, https://doi.org/10.1074/jbc.M107755200.

[14] R. Littlechild, N. Zaidman, D. Khodaverdi, M.J. Mason, Inhibition of KCa3.1 by depolarisation and 2-aminoethoxydiphenyl borate (2-APB) during Ca2+ release activated Ca2+ (CRAC) entry in human erythroleukemia (HEL) cells: implications for the interpretation of 2-APB inhibition of CRAC entry, Cell Calcium 57 (2015) 76–88, https://doi.org/10.1016/j.ceca.2014.12.009.

[15] M. Prakriya, R.S. Lewis, Store-operated calcium channels, Physiol. Rev. 95 (2015) 1383–1436, https://doi.org/10.1152/physrev.00020.2014.

[16] Y. Dobrydneva, C.J. Abelt, B. Dovel, C.M. Thadigiri, R.L. Williams, P.F. Blackmore, 2-aminoethoxydiphenyl borate as a prototype drug for a group of structurally related calcium channel blockers in human platelets, Mol. Pharmacol. 69 (2006) 247–256, https://doi.org/10.1124/mol.105.015701.

[17] H. Zhou, H. Iwasaki, T. Nakamura, K. Nakamura, T. Maruyama, S. Hamano, S. Ozaki, A. Mizutani, K. Mikoshiba, 2-Aminoethyl diphenylborinate analogues: selective inhibition for store-operated Ca2+ entry, Biochem. Biophys. Res. Commun. 352 (2007) 277–282, https://doi.org/10.1016/j.bbrc.2006.10.174.
[18] A.Z. Suzuki, S. Ozaki, J. Goto, K. Mikoshiba, Synthesis of bisboron compounds and their strong inhibitory activity on store-operated calcium entry, Bioorg. Med. Chem. Lett. 20 (2010) 1395–1398, https://doi.org/10.1016/j.bmcl.2009.12.108.
[19] J. Goto, A.Z. Suzuki, S. Ozaki, N. Matsumoto, T. Nakamura, E. Ebisui, A. Fleig, R. Penner, K. Mikoshiba, Two novel 2-aminoethyl diphenylborinate (2-APB) analogues differentially activate and inhibit store-operated Ca(2+) entry via STIM proteins, Cell Calcium 47 (2010) 1–10, https://doi.org/10.1016/j.ceca.2009.10.004.
[20] S. Ozaki, A.Z. Suzuki, P.O. Bauer, E. Ebisui, K. Mikoshiba, 2-Aminoethyl diphenylborinate (2-APB) analogues: regulation of Ca2+ signaling, Biochem. Biophys. Res. Commun. 441 (2013) 286–290, https://doi.org/10.1016/j.bbrc.2013.08.102.
[21] A. Hofer, G. Kovacs, A. Zappatini, M. Leuenberger, M.A. Hediger, M. Lochner, Design, synthesis and pharmacological characterization of analogs of 2-aminoethyl diphenylborinate (2-APB), a known store-operated calcium channel blocker, for inhibition of TRPV6-mediated calcium transport, Bioorg. Med. Chem. 21 (2013) 3202–3213, https://doi.org/10.1016/j.bmc.2013.03.037.
[22] A. Schild, R. Bhardwaj, N. Wenger, D. Tscherrig, P. Kandasamy, J. Dernic, R. Baur, C. Peinelt, M.A. Hediger, M. Lochner, Synthesis and pharmacological characterization of 2-aminoethyl diphenylborinate (2-APB) derivatives for inhibition of store-operated calcium entry (SOCE) in MDA-MB-231 breast cancer cells, Int. J. Mol. Sci. 21 (2020) 5604, https://doi.org/10.3390/ijms21165604.
[23] L. Gao, P. Yang, P. Qin, Y. Lu, X. Li, Q. Tian, Y. Li, C. Xie, J.B. Tian, C. Zhang, C. Tian, M.X. Zhu, J. Yao, Selective potentiation of 2-APB-induced activation of TRPV1-3 channels by acid, Sci. Rep. 6 (2016), 20791, https://doi.org/10.1038/srep20791.
[24] R.A. Clemens, C.A. Lowell, CRAC channel regulation of innate immune cells in health and disease, Cell Calcium 78 (2019) 56–65, https://doi.org/10.1016/j.ceca.2019.01.003.
[25] J. Hann, J.L. Bueb, F. Tolle, S. Brechard, Calcium signaling and regulation of neutrophil functions: still a long way to go, J. Leukoc. Biol. 107 (2020) 285–297, https://doi.org/10.1002/JLB.3RU0719-241R.
[26] S. Brechard, C. Melchior, S. Plancon, V. Schenten, E.J. Tschirhart, Store-operated Ca2+ channels formed by TRPC1, TRPC6 and Orai1 and non-store-operated channels formed by TRPC3 are involved in the regulation of NADPH oxidase in HL-60 granulocytes, Cell Calcium 44 (2008) 492–506, https://doi.org/10.1016/j.ceca.2008.03.002.
[27] J.D. Lambeth, Nox enzymes and the biology of reactive oxygen, Nat. Rev. Immunol. 4 (2004) 181–189, https://doi.org/10.1038/nri1312.
[28] K. Bedard, K.H. Krause, The NOX family of ROS-generating NADPH oxidases: physiology and pathophysiology, Physiol. Rev. 87 (2007) 245–313, https://doi.org/10.1152/physrev.00044.2005.
[29] S. Saul, C.S. Gibhardt, B. Schmidt, A. Lis, B. Pasieka, D. Conrad, P. Jung, R. Gaupp, B. Wonnenberg, E. Diler, H. Stanisz, T. Vogt, E.C. Schwarz, M. Bischoff, M. Herrmann, T. Tschernig, R. Kappl, H. Rieger, B.A. Niemeyer, I. Bogeski, A calcium-redox feedback loop controls human monocyte immune responses: the role of ORAI Ca2+ channels, Sci. Signal. 9 (2016) ra26, https://doi.org/10.1126/scisignal.aaf1639.
[30] I. Bogeski, C. Kummerow, D. Al-Ansary, E.C. Schwarz, R. Koehler, D. Kozai, N. Takahashi, C. Peinelt, D. Griesemer, M. Bozem, Y. Mori, M. Hoth, B. A. Niemeyer, Differential redox regulation of ORAI ion channels: a mechanism to tune cellular calcium signaling, Sci. Signal. 3 (2010) ra24, https://doi.org/10.1126/scisignal.2000672.
[31] S. Thierbach, N. Bui, J. Zapp, S.R. Chhabra, R. Kappl, S. Fetzner, Substrate-assisted O-2 activation in a cofactor-independent dioxygenase, Chem. Biol. 21 (2014) 217–225, https://doi.org/10.1016/j.chembiol.2013.11.013.
[32] S.I. Dikalov, I.A. Kirilyuk, M. Voinov, I.A. Grigor'ev, EPR detection of cellular and mitochondrial superoxide using cyclic hydroxylamines, Free Radic. Res. 45 (2011) 417–430, https://doi.org/10.3109/10715762.2010.540242.
[33] S.I. Dikalov, Y.F. Polienko, I. Kirilyuk, Electron Paramagnetic Resonance Measurements of Reactive Oxygen Species by Cyclic Hydroxylamine Spin Probes, Antioxidants & Redox Signaling, 2017, https://doi.org/10.1089/ars.2017.7396.
[34] O. Thastrup, P.J. Cullen, B.K. Drobak, M.R. Hanley, A.P. Dawson, Thapsigargin, a tumor promoter, discharges intracellular CA-2+ stores by specific-inhibition of the endoplasmic-reticulum CA-2+-ATPASE, Proc. Natl. Acad. Sci. U.S.A. 87 (1990) 2466–2470, https://doi.org/10.1073/pnas.87.7.2466.
[35] R. Balz, U. Brandle, E. Kammerer, D. Kohnlein, O. Lutz, A. Nolle, R. Schafitel, E. Veil, B-11 and B-10 NMR investigations in aqueous-solutions, Zeitschrift Fur Naturforschung Section a-a Journal of Physical Sciences 41 (1986) 737–742, https://doi.org/10.1515/zna-1986-0508.
[36] H.G. Kuivila, A.G. Armour, Electrophilic displacement reactions .9. Effects of substituents on rates of reactions between hydrogen peroxide and benzeneboronic acid, J. Am. Chem. Soc. 79 (1957) 5659–5662, https://doi.org/10.1021/ja01578a020.
[37] H.G. Kuivila, Electrophilic displacement reactions .3. Kinetics of the reaction between hydrogen peroxide and benzeneboronic acid, J. Am. Chem. Soc. 76 (1954) 870–874, https://doi.org/10.1021/ja01632a070.
[38] S. Brechard, E.J. Tschirhart, Regulation of superoxide production in neutrophils: role of calcium influx, J. Leukoc. Biol. 84 (2008) 1223–1237, https://doi.org/10.1189/jlb.0807553.
[39] D. Bakowski, M.D. Glitsch, A.B. Parekh, An examination of the secretion-like coupling model for the activation of the Ca2+ release-activated Ca2+ current I-CRAC in RBL-1 cells, J. Physiol.-London 532 (2001) 55–71, https://doi.org/10.1111/j.1469-7793.2001.0055g.x.
[40] B. Qu, D. Al-Ansary, C. Kummerow, M. Hoth, E.C. Schwarz, ORAI-mediated calcium influx in T cell proliferation, apoptosis and tolerance, Cell Calcium 50 (2011) 261–269, https://doi.org/10.1016/j.ceca.2011.05.015.
[41] A. Jairaman, M. Prakriya, Molecular pharmacology of store-operated CRAC channels, Channels 7 (2013) 402–414, https://doi.org/10.4161/chan.25292.
[42] Q. Yang, Y. Li, J.D. Yang, Y.D. Liu, L. Zhang, S.Z. Luo, J.P. Cheng, Holistic prediction of the pK(a) in diverse solvents based on a machine-learning approach, Angew. Chem.-Int. Edit. 59 (2020) 19282–19291, https://doi.org/10.1002/anie.202008528.
[43] Y.J. Shiao, J.E. Vance, Evidence for an ethanolamine cycle - differential recycling of the ethanolamine moiety of phosphatidylethanolamine derived from phosphatidylserine and ethanolamine, Biochem. J. 310 (1995) 673–679, https://doi.org/10.1042/bj3100673.
[44] M.G. Chudzinski, Y.C. Chi, M.S. Taylor, Borinic acids: a neglected class of organoboron compounds for recognition of diols in aqueous solution, Aust. J. Chem. 64 (2011) 1466–1469, https://doi.org/10.1071/ch11294.
[45] H. Morihara, M. Obana, S. Tanaka, I. Kawakatsu, D. Tsuchiyama, S. Mori, H. Suizu, A. Ishida, R. Kimura, I. Tsuchimochi, M. Maeda, T. Yoshimitsu, Y. Fujio, H. Nakayama, 2-aminoethoxydiphenyl borate provides an anti-oxidative effect and mediates cardioprotection during ischemia reperfusion in mice, PLoS One 12 (2017), e0189948, https://doi.org/10.1371/journal.pone.0189948.
[46] D. Conrad, PhD Dissertation, Universtät des Saarlandes, 2019.
[47] E. Aldieri, C. Riganti, M. Polimeni, E. Gazzano, C. Lussiana, I. Campia, D. Ghigo, Classical inhibitors of NOX NAD(P) H oxidases are not specific, Curr. Drug Metabol. 9 (2008) 686–696, https://doi.org/10.2174/138920008786049285.